THE JOURNAL OF PHYSICAL CHEMISTRY C

Article

pubs.acs.org/JPCC

Identifying Highly Conducting Au−C Links through Inelastic Electron Tunneling Spectroscopy

Giuseppe Foti,*[,†,‡] Héctor Vázquez,[§] Daniel Sánchez-Portal,[†,‡] Andrés Arnau,[†,‡,∥] and Thomas Frederiksen[‡,⊥]

[†]Centro de Física de Materiales, Centro Mixto CSIC-UPV/EHU, Paseo Manuel de Lardizabal 5, E-20018 Donostia-San Sebastián, Spain

[‡]Donostia International Physics Center (DIPC), Paseo Manuel de Lardizabal 4, E-20018 Donostia-San Sebastián, Spain

[§]Institute of Physics, Academy of Sciences of the Czech Republic, Cukrovarnicka 10, Prague CZ-162 00, Czech Republic

[∥]Depto. de Física de Materiales UPV/EHU, Facultad de Química, Apdo. 1072, E-20080 Donostia-San Sebastián, Spain

[⊥]IKERBASQUE, Basque Foundation for Science, E-48013 Bilbao, Spain

ABSTRACT: We use inelastic electron tunneling spectroscopy first-principles simulations to identify the different chemical bonds present at metal−molecule junctions. We unambiguously identify the nature of these bonds from two distinctive features in the calculated spectra: (i) the presence (or absence) of active vibrational modes and (ii) the dependence of vibrational frequencies on electrode separation. We use this method to present a study of the vibrational properties of alkanes bound to the electrodes via highly conducting Au−C links. In the experiment, these links were formed from molecules synthesized with trimethyl-tin ($SnMe_3$) terminations, where the $SnMe_3$ groups were removed in situ at the junction, in a process involving both breaking and formation of bonds [Cheng, Z.-L.; Skouta, R.; Vázquez, H.; Widawsky, J. R.; Schneebeli, S.; Chen, W.; Hybertsen, M. S.; Breslow, R.; Venkataraman, L. *Nat. Nanotechnol.* **2011**, *6*, 353−357]. We obtain the vibrational fingerprint of these direct Au−alkane links and extend this study to the other scenario considered in that paper (bonding via $SnMe_2$ groups), which may be relevant under other experimental conditions. We also explore the effect of deuteration on inelastic electron tunneling spectroscopy (IETS). Complete deuteration of the molecules diminishes the differences of the spectra corresponding to the two bonding geometries, making identification more difficult. IETS of an isolated $SnMe_3$ fragment provides an additional basis for comparison in the characterization of the molecular junction.

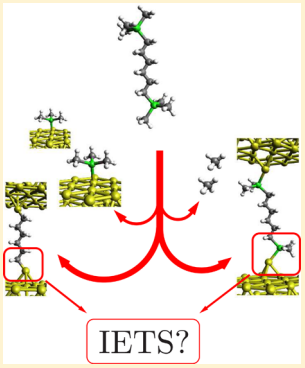

INTRODUCTION

The flow of an electrical current through molecules has been studied extensively over the past decades due to its fundamental interest and its importance in many physical, chemical, and biological processes.[1] These molecules are often prepared with chemical end groups which bind to the metal electrodes, forming stable and well-defined contacts for the molecular circuit. Thiol[2] and amine[3] groups are the most prevalent in single-molecule transport studies. At the same time, however, other link groups are being explored since metal−molecule links strongly influence the geometric and conducting properties of the molecular junction.[4,5] Recently, highly conducting Au−C links for single molecule transport were demonstrated.[6,7] For alkanes, the measured conductance was almost ∼100 times higher than that with other terminations. These molecules were initially synthesized with trimethyl tin ($SnMe_3$) end groups. It was shown[6,7] that the $SnMe_3$ groups were detached in situ at the junction, resulting in the formation of covalent Au−C bonds. However, unlike molecules having other linkers,[2−5] $SnMe_3$-terminated alkanes undergo both the breaking of molecular bonds as well as the formation of new bonds between electrode and molecule. This process of in situ breaking and formation of bonds that led to Au−C links has not yet been studied in detail. Therefore, one cannot, in principle, rule out the occurrence of other bond breaking and formation processes under different experimental conditions (e.g., in ultrahigh vacuum or at low temperature). In particular, in ref 6, the authors initially considered another binding scenario, where only a methylene group (and not the whole $SnMe_3$) was removed at each end and the alkane backbone was bonded via $SnMe_2$ links.

Inelastic electron tunneling spectroscopy (IETS) is ideally suited to address this issue, due to its ability to identify molecular species at nanojunctions that has resulted in its use in chemical analysis of single molecules.[8−10] In this paper, we use IETS to unambiguously identify the different bonds present at the molecular junction. We predict the vibrational signature of the two scenarios considered in ref 6 for the in situ formation of metal−molecule bonds: (i) cleavage of the whole $SnMe_3$ groups and direct binding of Au to the alkane backbone, and

Received: August 1, 2014
Revised: October 20, 2014
Published: October 21, 2014

   dx.doi.org/10.1021/jp5077824 | *J. Phys. Chem. C* 2014, 118, 27106−27112

(ii) scission of one CH_3 group from each Sn atom and binding of the alkane backbone through $SnMe_2$ links. The different metal−molecule links in these scenarios give rise to distinctive features in the IETS signals, which allow us to chemically characterize the junction and unambiguously identify the conducting molecular species. We expect this work to be useful in the study of the in situ formation of highly conducting links as it predicts the vibrational signatures associated with the presence of the different bonds (e.g., Sn−C, Sn−Au, or Au−C) that can be formed from $SnMe_3$ molecules. Moreover, since the vibrational properties of alkanes bound via direct Au−C links (scenario (i)) have not been, to the best of our knowledge, investigated before, our results represent the first study of the IETS signature of alkanes having highly conducting Au−C links.

METHODS

Figure 1 shows the isolated $SnMe_3$-terminated hexane molecule (C6, Figure 1a) as well as the two considered binding scenarios

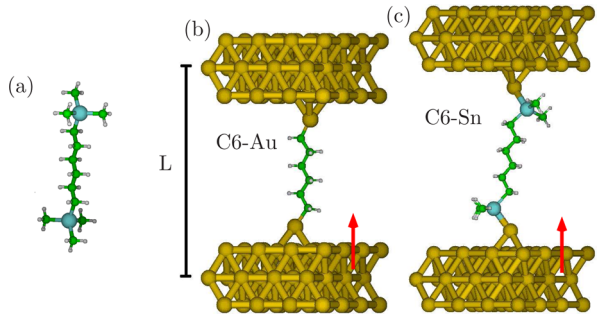

Figure 1. (a) C6 molecules initially synthesized with $SnMe_3$ groups. (b) Scenario with direct Au−C covalent bonds resulting from the cleavage of $SnMe_3$ groups. (c) Bonding through $SnMe_2$ links after scission of a methyl group. L defines the electrode separation and is measured between the (fixed) second Au layers at both sides of the junction. C atoms, green; Sn, blue; H, white; Au, yellow. Red arrow indicates the direction of electron flow for $V > 0$.

to the gold electrodes: direct Au−C bonds (C6−Au, Figure 1 b) or bonding via $SnMe_2$ groups (C6−Sn, Figure 1c). We calculate the junction structure and its transmission properties using the SIESTA/TranSIESTA[11,12] codes based on density functional theory (DFT). We use the Inelastica[13,14] package to calculate the vibrational modes, electron-vibration couplings M^{λ}, and IETS spectra. We use a single-ζ polarized basis for gold (Au) and a double-ζ polarized basis for hydrogen (H), carbon (C), and tin (Sn) atoms. Also, for the atoms of the outermost gold surface, we use a diffuse orbitals basis.[15] For gold, we use a lattice constant a = 4.14 Å, corresponding to the relaxed lattice parameter with the calculation parameters used here. All calculations are performed in the generalized gradient approximation.[16] The real-space grid is fixed at 250 Ry, while a $k = 5 \times 5 \times 1$ Monkhorst−Pack mesh is used for the sampling of k-space. For each electrode−electrode separation, we relax the position of the atoms in the molecule, adatoms, and the first gold layer until residual forces are below 0.02 eV/Å. At each distance, transmission at the Fermi level is calculated with a k-point sampling of $k = 15 \times 15$. The dynamical region for the calculation of electron-vibration coupling includes the molecule and the gold adatoms. IETS signals were calculated in the wide band approximation[17] as an average over electron momentum[18] with a k-grid of 10×10.

The IETS signals in Figure 3 are calculated using a modulation voltage V_{rms} = 5 meV[13,14] and are consistent with results using other V_{rms} values. For a range of electrode−electrode distances, we calculate the vibrational fingerprints of both bonding scenarios using IETS, defined in the usual way as the ratio $(d^2I/dV^2)/(dI/dV)$ between the second and first derivatives of the tunnel current I with respect to the applied bias V. We start at the energy minimum with respect to the electrode separation and increase the distance between electrodes in steps of 0.5 Å for a total of 2 Å to reproduce the experimental conditions in molecular traces.

RESULTS

Concerning the elastic transport properties, we find that the calculated conductance of C6−Au is approximately an order of magnitude higher than that of C6−Sn. Unlike the case of thiol-functionalized alkanes, for which it has been reported that stretching the junction induces an increase of the conductance,[19−22] our results show that, for both pure and tin-functionalized alkanes, the transmission around the Fermi energy decreases almost linearly with increasing electrodes separation (Figure 2). We relate this to the reduction of the electronic coupling between metal and molecular states upon stretching.

The IETS curves for C6−Au and C6−Sn are shown in Figure 3. The IETS signals in the 50−200 meV range and their dependence on electrode separation show differences which allow us to clearly distinguish between Au−C and Au−Sn bound junctions. In general, a clear signal in the IETS of alkane chains arises from C−H and C−C modes[19,23−30] while low-energy peaks are associated with the heavier gold and tin atoms.

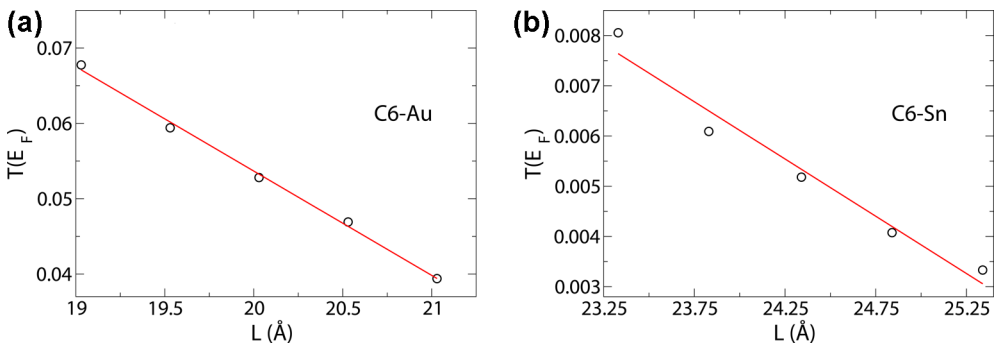

Figure 2. Transmission coefficient at the Fermi level as a function of stretching for (a) C6−Au and (b) C6−Sn. The red curves are linear fits with slopes −0.013 and −0.0022 $Å^{-1}$ for C6−Au and C6−Sn, respectively.

dx.doi.org/10.1021/jp5077824 | J. Phys. Chem. C 2014, 118, 27106−27112

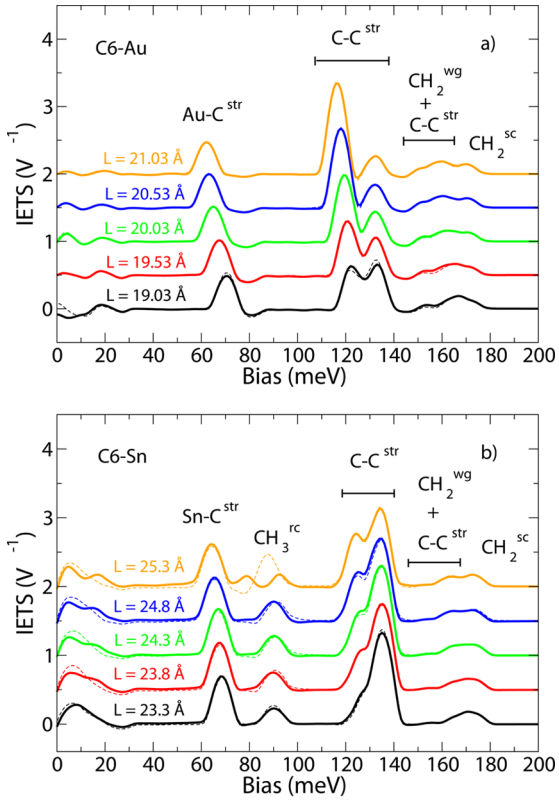

Figure 3. Calculated IETS of (a) C6−Au and (b) C6−Sn for five different electrode separations. For clarity, these curves are shifted by 0.5 V^{-1}. For each geometry, the spectra for positive (negative) voltages are shown in solid (dashed) lines. The labels indicate different vibrational modes (str = stretch, rc = rock, wg = wag, sc = scissor).

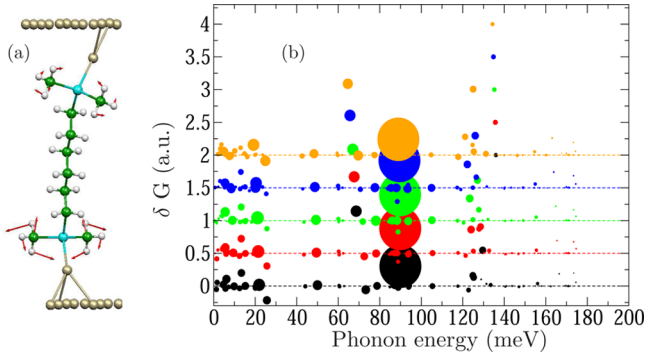

Figure 4. (a) Probe vector constructed by considering the movement of just the methyl groups. (b) Mode-resolved change in the conductance δG for C6−Sn. The radius of the filled circles is proportional to the projections over the probe mode. Colors indicate different stretching conditions according to the convention adopted in Figure 3. Data corresponding to different stretching conditions are offset for clarity. The horizontal lines indicate the baseline (zero δG) of each calculation.

Features below ~25 meV are typically related to the Au atoms.[13]

The labels in Figure 3 describe the vibrational modes giving rise to a particular peak or group of peaks. In the case of C6−Au, the low-energy peak around 70 meV is given by the Au−C^{str} stretching mode. The frequency is smaller than the typical S−C^{str} stretching mode in alkanethiol-based junctions[19,28,30] where it is usually found between 80 and 90 meV. In the case of C6−Sn, a similar IETS peak is also found around 70 meV but corresponding to the Sn−C^{str} mode. The vibrational signature of the Au−Sn mode, which lies below ~25 meV, does not appear clearly in the IETS curve. The features in the 120−135 meV region can be described for both C6−Au and C6−Sn in terms of C−C^{str} stretching modes. Between 140 and 150 meV, the main contributions come from CH_2 wag modes (CH_2^{wg}) while the peak at 170 meV is given by CH_2 scissor modes (CH_2^{sc}).

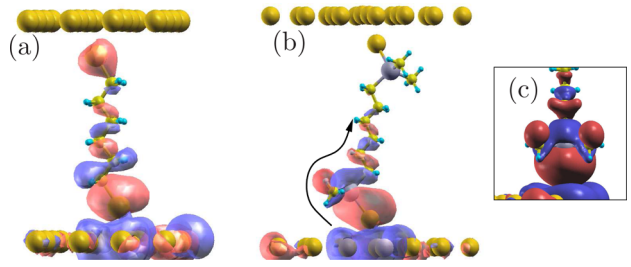

Figure 5. Side view of the most transmitting eigenchannels for (a) C6−Au and (b) C6−Sn junctions corresponding to scattering states incoming from below. In both cases, the eigenchannels are of σ symmetry. (c) Front view of the scattering state of C6−Sn also visualized in panel (b).

Table 1. Softening Rate ($d\hbar\omega/dL$) of Low Energy Peaks with Respect to Increasing Electrode Separation for the C6−Au and C6−Sn Junctions[a]

molecule	mode freq (meV)	$d\hbar\omega/dL$ (meV/Å)	mode description
C6−Au	62	−4.0	Au−C^{str}
	122	−2.7	C−C^{str}
	133	−0.9	C−C^{str}
	155	−1.3	C−C^{wg} + C−C^{str}
	163	−4.1	C−C^{wg} + C−C^{str}
C6−Sn	64	−2.0	Sn−C^{str}
	90	−0.6	CH_3^{rc}
	125	−0.9	C−C^{str}
	135	−0.3	C−C^{str}
	155	−0.6	C−C^{wg} + C−C^{str}
	163	−1.6	C−C^{wg} + C−C^{str}

[a]The second column represents the position of the peak at the equilibrium distance L_0.

At first glance, our computed IETS curve thus appear rather similar to features of alkanes reported in the literature.[19,27−29] Upon close inspection, the IETS curves of C6−Au and C6−Sn present important differences, in particular, around 90 meV where the CH_3^{rc} rock mode, previously reported to be active,[29] indeed gives a signal only for C6−Sn.

To quantify the vibrational character of the different signals in IETS, we project the vibrational modes Φ_i onto well-characterized probe vectors p. As an example, we constructed the probe vector shown in Figure 4a with pure CH_3 rock motion (constructed by considering the movement of just the methyl groups). Figure 4b then reveals simultaneously for each vibrational mode its CH_3 rock character (symbol radius proportional to the projections) as well as its contribution to the IETS intensity (y-axis proportional to the conductance change δG_i over the emission threshold). Clearly, the mode at 90 meV is well characterized as CH_3 rock and it leaves a considerable signal in IETS.

dx.doi.org/10.1021/jp5077824 | J. Phys. Chem. C 2014, 118, 27106−27112

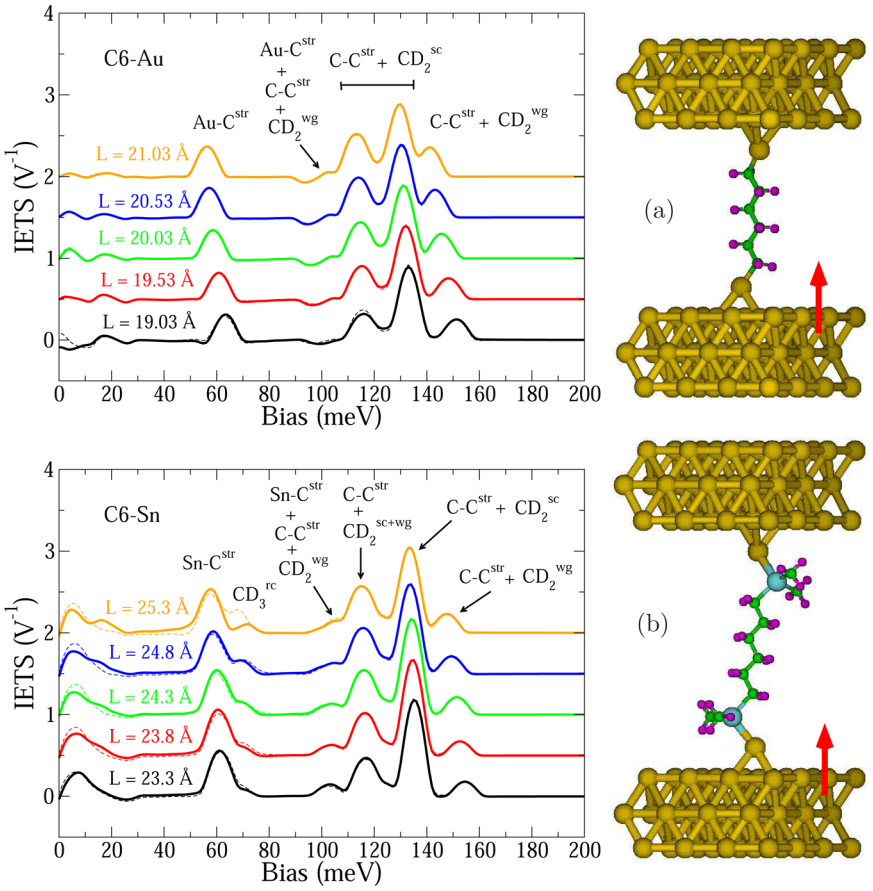

Figure 6. IET spectra of the fully deuterated (a) C6−Au and (b) C6−Sn molecules in the L_0 geometry. Deuterium atoms are marked in violet. For each geometry, the spectra for positive (negative) voltages are shown in solid (dashed) lines. Red arrow indicates the direction of electron flow for $V > 0$.

For C6−Au, no features are found in IETS in this energy range since there are no CH_3 groups bound to the conducting backbone. The CH_3 signal is therefore a signature of $SnMe_2$-bound junctions and thus allows us to unambiguously discriminate between the two binding scenarios.

A slight asymmetry in IETS with respect to bias polarity develops in C6−Sn junctions with increasing electrode separation. This originates from the geometric asymmetry in the orientation of the $SnMe_2$ groups (Figure 4b), which primarily affects the rock mode of the CH_3 groups.

The relative amplitude of the peaks shown in Figure 3 can be rationalized in terms of the matrix elements $|\langle\Psi_{f,n}|M^{\lambda}|\Psi_{i,m}\rangle|^2$ between initial ($\Psi_{i,m}$) and final ($\Psi_{f,n}$) scattering states together with the electron-vibration couplings M^{λ}.[31] For both C6−Au and C6−Sn, we have one main transmission eigenchannel[32] with rotational (σ-type) symmetry with respect to the electron tunneling pathway (Figure 5). Electron waves incoming from either electrode decay exponentially through the molecular backbone as expected from the tunneling conditions. The propensity rules[31] hence favor longitudinal modes with respect to the transport axis, such as the C−C, Au−C, and Sn−C stretch modes.

Interestingly, although the CH_3 rocking mode does not involve the carbon backbone of the molecule, it still gives an appreciable contribution to IETS. The eigenchannel plots (Figure 5) reveal that the scattering state of C6−Sn has a significant amplitude on the methyl groups attached to the Sn atom. This is consistent with the deformation potential associated with the CH_3 mode at 90 meV having a nonzero overlap with scattering states on both sides of the molecule and resulting in a peak in the IETS curves.

Dependence of IETS on Electrode Separation. We now discuss the dependence of the dominant IETS peaks as a function of electrode separation,[19,26,33,34] since it provides another means to clearly distinguish between C6−Au and C6−Sn junctions. Table 1 shows the stretching dependence ($d\hbar\omega/dL$) for the two considered bonding scenarios, calculated as the fit to the peak maxima over the five electrode separations considered and averaged over positive and negative bias. The Au−C^{str} peak of C6−Au shifts significantly upon junction stretching, having a red shift of 8 meV over a 2 Å increase. For C6−Sn, the Sn−C^{str} peak moves down by only 4 meV over the same electrode separation range. This is in part due to the fact that the C6−Sn junction is longer than C6−Au, which distributes the stretching among more bonds, and in part due also to the stiffness of the different (Au−Sn, Sn−C, and Au−C) chemical bonds. The softening rate of the modes with C−C^{str} character is three times higher for C6−Au than for C6−Sn junctions. The small peak at 165 meV resulting from CH_2^{wg} and C−C^{str} modes splits in two contributions for both C6−Au and C6−Sn. The splitting with electrode separation is roughly the double for C6−Au than for C6−Sn.

Finally, the signal from the CH_3 modes at 90 meV (for the C6−Sn junction) displays a rather weak distance dependence. From our calculations, we thus see that the dependence of IETS peak position on electrode separation is much stronger

dx.doi.org/10.1021/jp5077824 | J. Phys. Chem. C 2014, 118, 27106−27112

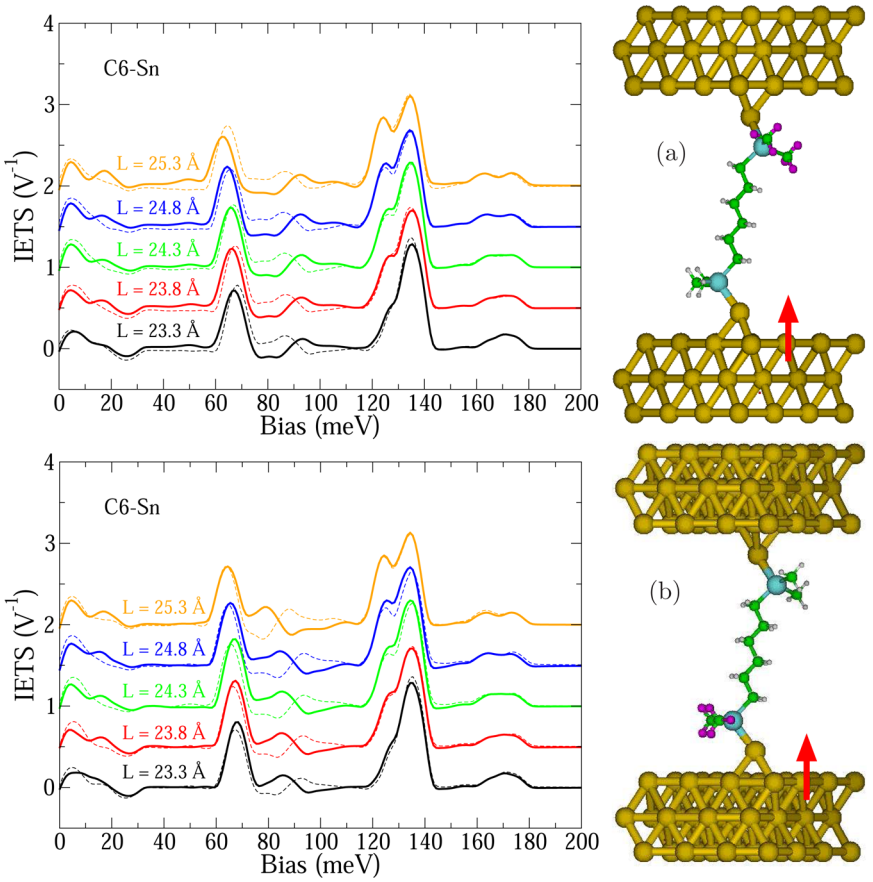

Figure 7. (a) IET spectra of C6−Sn after deuteration of the upper and lower methyl groups (b). For each geometry, the spectra for positive (negative) voltages are shown in solid (dashed) lines. Red arrow indicates the direction of electron flow for $V > 0$.

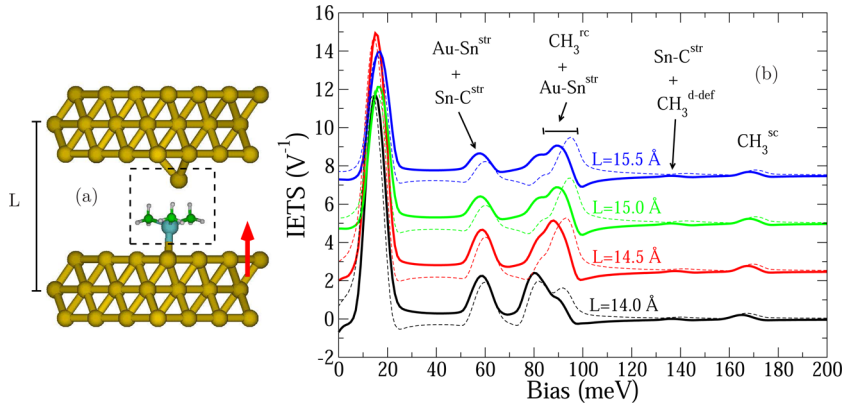

Figure 8. (a) Side view of the $SnMe_3$ fragment at $L = 14.0$ Å and (b) IET spectra of the $SnMe_3$ fragment at four different electrode separations. For each geometry, the spectra for positive (negative) voltages are shown in solid (dashed) lines. Red arrow indicates the direction of electron flow for $V > 0$.

for C6−Au than for C6−Sn. This points to a second mechanism by which to discriminate the composition of the molecular junction: quantifying the peak shifts in the IETS signal with electrode separation.[19]

IETS of Deuterated Molecules. We now turn to the effect of deuteration on the IETS curves. Figure 6 shows the IET spectra of the fully deuterated molecules. For both C6−Au and C6−Sn, we see a down-shift of all peaks associated with CH_2 modes, which now mix with C−C stretching modes. The peak at 135 meV remains at the same position in both cases but now it is a combination of C−C^{str} and CD_2^{sc} modes. For both C6−Au and C6−Sn, two additional peaks appear slightly above 100 meV and at 117 meV. In the 110−160 meV energy range, in addition to the C−C^{str} modes, we now find CD_2^{wg} and CD_2^{sc} modes.

The most relevant result is that the C6−Sn peak associated with the CH_3^{rc} mode merges with the Sn−C^{str} peak. Thus, complete deuteration diminishes the differences in IETS of the two different bonding scenarios, making identification more difficult.

In contrast, selective deuteration of the CH_3 groups attached to only *one* of the two Sn atoms in C6−Sn gives rise to a

dx.doi.org/10.1021/jp5077824 | J. Phys. Chem. C 2014, 118, 27106−27112

pronounced asymmetry in the IETS signal arising from the CD_3^{rc} mode (Figure 7). We note that this asymmetry may be used as an additional tool to identify the C6−Sn junction.

IETS of the $SnMe_3$ Fragment. In order to provide a complete characterization of both binding scenarios, we calculate the inelastic signal expected in the case where the $SnMe_3$ fragments separate from the alkane chain. Energetic and entropic arguments[6] suggested that the $SnMe_3$ fragments adsorb on the Au surface. Here we predict its vibrational features for future experimental (e.g., low-temperature STM) studies. We show that this fragment would give a very different inelastic spectrum compared to that of both C6−Au and C6−Sn. Figure 8a shows the side view of the junction geometry for L = 14.0 Å, where the dashed line encloses the dynamical region. Figure 8b shows the IET spectra at four different electrode separations. The asymmetry in the low energy part of the spectrum with respect to bias polarity is due to the asymmetry of the molecular junction.

The $SnMe_3$ group gives a clear IETS signal. At ∼ 60 meV there is a feature arising from the $Au-Sn^{str}$ and $Sn-C^{str}$ modes. The peak resulting from the CH_3^{rc} mode appears around 80 meV, slightly lower than in the case of C6−Sn. For $SnMe_3$ there are no C−C bonds and the (small) signal present between 120 and 144 meV is due to a combination of Sn−C stretching and CH_3 d-deform modes.[28] The characterization of the IETS characteristics of the $SnMe_3$ fragment completes the analysis of the C6−Au scenario where the whole $SnMe_3$ groups are detached.

CONCLUSIONS

In summary, we carry out first-principles calculations of IETS to investigate and characterize junctions where alkanes synthesized with $SnMe_3$ groups are bound to Au. We consider two binding scenarios and obtain the vibrational fingerprints corresponding to the binding of the alkane backbone directly to Au or via $SnMe_2$ groups. The IETS curves of C6−Sn junctions show a peak around ∼90 meV arising from the CH_3 groups bound to Sn. The vibrational spectra of C6−Au junctions exhibit no features at this energy. In addition, the dependence on electrode separation of the IETS peaks is significantly stronger in the case of Au−C bonds than for $SnMe_2$-terminated molecules. Selective deuteration of the CH_3 groups at just *one* of the molecular terminations, though not complete deuteration, introduces a strong asymmetry in the IETS signals with respect to bias polarity. Finally, we obtain the vibrational fingerprint of the $SnMe_3$ fragment cleaved from the alkane chain during the formation of the Au−C bond. These differences allow us to unambiguously characterize both scenarios chemically and to provide important information on the different metal−molecule bonds present at molecular junctions.

AUTHOR INFORMATION

Corresponding Author

*E-mail: giuseppe_foti@ehu.es.

Notes

The authors declare no competing financial interest.

ACKNOWLEDGMENTS

H.V. acknowledges financial support from the Academy of Sciences of the Czech Republic through the J.E. Purkyně fellowship. G.F., D.S.-P., A.A., and T.F. acknowledge the support of the Basque Departamento de Educación and the UPV/EHU (Grant No. IT-756-13) and the Spanish Ministerio de Economía y Competitividad (Grant No. FIS2013-48286-C2-2-P and Grant No. MAT2013-46593-C6-2-P). D.S.-P. and T.F. acknowledge the European Union FP7-ICT project PAMS (Contract No. 610446).

REFERENCES

(1) Cuevas, J. C.; Scheer, E. *Molecular Electronics: An Introduction to Theory and Experiment*; World Scientific: Singapore, 2010.
(2) Reed, M. A.; Zhou, C.; Muller, C. J.; Burgin, T. P.; Tour, J. M. Conductance of a Molecular Junction. *Science* **1997**, *278*, 252−254.
(3) Venkataraman, L.; Klare, J. E.; Tam, I. W.; Nuckolls, C.; Hybertsen, M. S.; Steigerwald, M. L. Single-Molecule Circuits with Well-Defined Molecular Conductance. *Nano Lett.* **2006**, *6*, 458−462.
(4) Park, Y. S.; Whalley, A. C.; Kamenetska, M.; Steigerwald, M. L.; Hybertsen, M. S.; Nuckolls, C.; Venkataraman, L. Contact Chemistry and Single-Molecule Conductance: A Comparison Of Phosphines, Methyl Sulfides, and Amines. *J. Am. Chem. Soc.* **2007**, *129*, 15768−15769.
(5) Mowbray, D.; Jones, G.; Thygesen, K. Influence of Functional Groups On Charge Transport in Molecular Junctions. *J. Chem. Phys.* **2008**, *128*, 111103.
(6) Cheng, Z.-L.; Skouta, R.; Vázquez, H.; Widawsky, J. R.; Schneebeli, S.; Chen, W.; Hybertsen, M. S.; Breslow, R.; Venkataraman, L. In Situ Formation of Highly Conducting Covalent Au-C Contacts For Single-Molecule Junctions. *Nat. Nanotechnol.* **2011**, *6*, 353−357.
(7) Chen, W.; Widawsky, J. R.; Vázquez, H.; Schneebeli, S. T.; Hybertsen, M. S.; Breslow, R.; Venkataraman, L. Highly Conducting -Conjugated Molecular Junctions Covalently Bonded to Gold Electrodes. *J. Am. Chem. Soc.* **2011**, *133*, 17160−17163.
(8) Komeda, T. Chemical Identification and Manipulation of Molecules by Vibrational Excitation Via Inelastic Tunneling Process with Scanning Tunneling Microscopy. *Prog. Surf. Sci.* **2005**, *78*, 41−85.
(9) Sainoo, Y.; Kim, Y.; Okawa, T.; Komeda, T.; Shigekawa, H.; Kawai, M. Excitation of Molecular Vibrational Modes with Inelastic Scanning Tunneling Microscopy Processes: Examination through Action Spectra of cis-2-Butene on Pd(110). *Phys. Rev. Lett.* **2005**, *95*, 246102.
(10) Bocquet, M.-L.; Lesnard, H.; Lorente, N. Inelastic Spectroscopy Identification of STM-Induced Benzene Dehydrogenation. *Phys. Rev. Lett.* **2006**, *96*, 096101.
(11) Soler, J. M.; Artacho, E.; Gale, J. D.; García, A.; Junquera, J.; Ordejón, P.; Sánchez-Portal, D. The SIESTA Method for Ab Initio Order-N Materials Simulation. *J. Phys.: Condens. Matter* **2002**, *14*, 2745.
(12) Brandbyge, M.; Mozos, J.-L.; Ordejón, P.; Taylor, J.; Stokbro, K. Density-functional Method for Nonequilibrium Electron Transport. *Phys. Rev. B* **2002**, *65*, 165401.
(13) Frederiksen, T.; Paulsson, M.; Brandbyge, M.; Jauho, A.-P. Inelastic Transport Theory From First Principles: Methodology and Application to Nanoscale Devices. *Phys. Rev. B* **2007**, *75*, 205413.
(14) The Inelastica code is a freely available at http://sourceforge.net/projects/inelastica.
(15) García-Gil, S.; García, A.; Lorente, N.; Ordejón, P. Optimal Strictly Localized Basis Sets for Noble Metal Surfaces. *Phys. Rev. B* **2009**, *79*, 075441.
(16) Perdew, J. P.; Burke, K.; Ernzerhof, M. Generalized Gradient Approximation Made Simple. *Phys. Rev. Lett.* **1996**, *77*, 3865−3868.
(17) Paulsson, M.; Frederiksen, T.; Brandbyge, M. Modeling Inelastic Phonon Scattering in Atomic- and Molecular-Wire Junctions. *Phys. Rev. B* **2005**, *72*, 201101.
(18) Foti, G.; Sanchez-Portal, D.; Arnau, A.; Frederiksen, T. Role of k-point Sampling in the Supercell Approach to Inelastic Electron Tunneling Spectroscopy Simulations of Molecular Monolayers. In preparation.

(19) Arroyo, C. R.; Frederiksen, T.; Rubio-Bollinger, G.; Vélez, M.; Arnau, A.; Sánchez-Portal, D.; Agraït, N. Characterization of Single-Molecule Pentanedithiol Junctions by Inelastic Electron Tunneling Spectroscopy and First-Principles Calculations. *Phys. Rev. B* **2010**, *81*, 075405.
(20) Bruot, C.; Hihath, J.; Tao, N. Mechanically Controlled Molecular Orbital Alignment in Single Molecule Junctions. *Nat. Nanotechnol.* **2011**, *7*, 35−40.
(21) French, W. R.; Iacovella, C. R.; Rungger, I.; Souza, A. M.; Sanvito, S.; Cummings, P. T. Atomistic Simulations of Highly Conductive Molecular Transport Junctions Under Realistic Conditions. *Nanoscale* **2013**, *5*, 3654−3659.
(22) Saffarzadeh, A.; Demir, F.; Kirczenow, G. Mechanism of the Enhanced Conductance of A Molecular Junction Under Tensile Stress. *Phys. Rev. B* **2014**, *89*, 045431.
(23) Kushmerick, J. G.; Lazorcik, J.; Patterson, C. H.; Shashidhar, R.; Seferos, D. S.; Bazan, G. C. Vibronic Contributions to Charge Transport Across Molecular Junctions. *Nano Lett.* **2004**, *4*, 639−642.
(24) Paulsson, M.; Frederiksen, T.; Brandbyge, M. Inelastic Transport Through Molecules: Comparing First-Principles Calculations to Experiments. *Nano Lett.* **2006**, *6*, 258−262.
(25) Solomon, G. C.; Gagliardi, A.; Pecchia, A.; Frauenheim, T.; Di Carlo, A.; Reimers, J. R.; Hush, N. S. Understanding the Inelastic Electron-Tunneling Spectra of Alkanedithiols On Gold. *J. Chem. Phys.* **2006**, *124*, 094704.
(26) Hihath, J.; Arroyo, C. R.; Rubio-Bollinger, G.; Tao, N. J.; Agraït, N. Study of Electron-Phonon Interactions in A Single Molecule Covalently Connected to Two Electrodes. *Nano Lett.* **2008**, *8*, 1673−1678.
(27) Okabayashi, N.; Konda, Y.; Komeda, T. Inelastic Electron Tunneling Spectroscopy of an Alkanethiol Self-Assembled Monolayer Using Scanning Tunneling Microscopy. *Phys. Rev. Lett.* **2008**, *100*, 217801.
(28) Okabayashi, N.; Paulsson, M.; Ueba, H.; Konda, Y.; Komeda, T. Inelastic Tunneling Spectroscopy of Alkanethiol Molecules: High-Resolution Spectroscopy and Theoretical Simulations. *Phys. Rev. Lett.* **2010**, *104*, 077801.
(29) Okabayashi, N.; Paulsson, M.; Ueba, H.; Konda, Y.; Komeda, T. Site Selective Inelastic Electron Tunneling Spectroscopy Probed by Isotope Labeling. *Nano Lett.* **2010**, *10*, 2950−2955.
(30) Kim, Y.; Song, H.; Strigl, F.; Pernau, H.-F.; Lee, T.; Scheer, E. Conductance and Vibrational States of Single-Molecule Junctions Controlled by Mechanical Stretching and Material Variation. *Phys. Rev. Lett.* **2011**, *106*, 196804.
(31) Paulsson, M.; Frederiksen, T.; Ueba, H.; Lorente, N.; Brandbyge, M. Unified Description of Inelastic Propensity Rules for Electron Transport through Nanoscale Junctions. *Phys. Rev. Lett.* **2008**, *100*, 226604.
(32) Paulsson, M.; Brandbyge, M. Transmission Eigenchannels From Nonequilibrium Green's Functions. *Phys. Rev. B* **2007**, *76*, 115117.
(33) Djukic, D.; Thygesen, K. S.; Untiedt, C.; Smit, R. H. M.; Jacobsen, K. W.; van Ruitenbeek, J. M. Stretching Dependence of the Vibration Modes of a Single-Molecule Pt-H-2-Pt Bridge. *Phys. Rev. B* **2005**, *71*, 161402.
(34) Kim, Y.; Pietsch, T.; Erbe, A.; Belzig, W.; Scheer, E. Benzenedithiol: A Broad-Range Single-Channel Molecular Conductor. *Nano Lett.* **2011**, *11*, 3734−3738.